JPET Fast Forward. Published on August 21, 2013 as DOI: 10.1124/jpet.113.205799

J. Pharmacol. Exp. Ther. - ***revised***
August 7, 2013

Biaryl amides and hydrazones as therapeutics for prion disease in transgenic mice

Duo Lu, Kurt Giles, Zhe Li[‡], Satish Rao, Elena Dolghih, Joel R. Gever, Michal Geva, Manuel Elepano, Abby Oehler, Clifford Bryant, Adam Renslo, Matthew P. Jacobson, Stephen J. DeArmond, B. Michael Silber, and Stanley B. Prusiner

Institute for Neurodegenerative Diseases (D.L., K.G., Z.L., S.R., J.R.G., M.G., M.E., S.J.D., B.M.S., S.B.P), Department of Neurology (K.G., Z.L., S.R., J.R.G., B.M.S., S.B.P.), Department of Pathology (A.O., S.J.D), Department of Pharmaceutical Chemistry (E.D., C.B., A.R., M.P.J.), and Small Molecule Discovery Center (C.B., A.R.), University of California San Francisco, CA 94143, U.S.A.

JPET Fast Forward. Published on August 21, 2013 as DOI: 10.1124/jpet.113.205799
This article has not been copyedited and formatted. The final version may differ from this version.

Running title: Prion therapeutics and bioluminescence imaging

Please address all correspondence to Stanley B. Prusiner at 675 Nelson Rising Lane, San Francisco, CA 94143-0518; Tel: (415) 476-4482; Fax: (415) 476-8386; e-mail: stanley@ind.ucsf.edu.

Number of text pages: 44
Number of tables: 3
Number of figures: 7
Number of references: 46
Number of words in the Abstract: 215
Number of words in the Introduction: 578
Number of words in the Discussion: 973

Abbreviations: PrP, prion protein; Tg, transgenic; Mo, mouse; GFAP, glial fibrillary acidic protein; PK, proteinase K; BLI, bioluminescence imaging.

Section: Drug Discovery and Translational Medicine

JPET Fast Forward. Published on August 21, 2013 as DOI: 10.1124/jpet.113.205799
This article has not been copyedited and formatted. The final version may differ from this version.

ABSTRACT

The only small-molecule compound demonstrated to substantially extend survival in prion-infected mice is a biaryl hydrazone termed “Compd B.” However, the hydrazone moiety of Compd B results in toxic metabolites, making it a poor candidate for further drug development. We developed a pharmacophore model based on diverse antiprion compounds identified by high-throughput screening and based on this model, we generated biaryl amide analogs of Compd B. Medicinal chemistry optimization led to multiple compounds with increased potency, increased brain concentrations, and greater metabolic stability, indicating that they could be promising candidates for antiprion therapy. Replacing the pyridyl ring of Compd B with a phenyl group containing an electron-donating substituent increased potency, while adding an aryl group to the oxazole moiety increased metabolic stability. To test the efficacy of Compd B, we applied bioluminescence imaging (BLI), which was previously shown to detect prion disease onset in live mice earlier than clinical signs. In our studies, Compd B showed good efficacy in two lines of transgenic mice infected with mouse-adapted RML prions, but not in transgenic mice infected with human prions. The BLI system successfully predicted the efficacies in all cases long before extension in survival could be observed. Our studies suggest that this BLI system has good potential to be applied in future antiprion drug efficacy studies.

JPET Fast Forward. Published on August 21, 2013 as DOI: 10.1124/jpet.113.205799
This article has not been copyedited and formatted. The final version may differ from this version.

INTRODUCTION

Prion diseases are a class of progressive and uniformly fatal neurodegenerative disorders, which include Creutzfeldt-Jakob disease (CJD) in humans, bovine spongiform encephalopathy (BSE) in cattle, chronic wasting disease (CWD) in elk and deer, and scrapie in sheep (Prusiner, 2007; Aguzzi et al., 2008). The vast majority (~85%) of CJD cases occur sporadically, but over 40 point mutations and octarepeat expansions have been identified in the prion protein (PrP) that cause familial prion diseases, which account for ~15% of cases; additionally, a small subset (<1%) of human PrP prion diseases have occurred through infection. Conversely, BSE, CWD, and scrapie are predominantly spread through an infectious etiology, although a genetic case of BSE has also been observed (Richt and Hall, 2008) and the periodic identification of new BSE cases likely represent spontaneous occurrences. All prion diseases result from refolding of the endogenous cellular prion protein (PrP^{C}) into a self-propagating form, denoted PrP^{Sc} (Prusiner, 1998). Stochastic refolding likely accounts for sporadic and genetic cases, whereas the infectious etiology results from an exogenous PrP^{Sc} nidus initiating template-dependent refolding of PrP^{C}. Currently, no treatments exist that halt or even slow any prion disease.

Numerous compounds have been reported to show antiprion activity in prion-infected cell-culture models, including pentosan polysulfate (PPS), dextran sulfate, heteropolyanion-23, Congo red, quinacrine, and 2-aminothiazoles (for a comprehensive review, see (Trevitt and Collinge, 2006; Sim, 2012)). However, the only small molecule demonstrated to substantially extend survival in prion-infected mice is “Compound B” (Kawasaki et al., 2007), hereafter referred to as “Compd B.”

Despite its low effective concentration (EC_{50}) *in vitro*, advancement of Compd B as a promising drug candidate is limited by the high-liability aryl hydrazone moiety present in its structure (Hwu et al., 2004). Therefore, we developed analogs of Compd B guided by a pharmacophore model, and generated more potent compounds with lower EC_{50} values. Pharmacokinetic studies conducted on these analogs indicated that several may prove to be suitable candidates as antiprion therapeutics.

While developing safe and more effective compounds for antiprion treatment, we were also seeking for novel methods to monitor and predict drug efficacy in mouse models. Currently, the only method to determine efficacy of candidate compounds *in vivo* is to compare survival times of treated and untreated prion-infected mice. Because wild-type mice generally have incubation periods of at least ~120–150 days, such studies are time consuming and expensive. Previously, we showed that bioluminescence imaging (BLI), using transgenic (Tg) mice expressing a luciferase (luc) reporter driven by the glial fibrillary acidic protein (GFAP) promoter, enabled prion disease progression to be monitored *in vivo*. Tg(*Gfap*-luc) mice showed upregulation of the BLI signal at ~60 days postinoculation (dpi) with RML prions, approximately half the time to onset of clinical signs (Tamgüney et al., 2009). In this study, we applied the BLI technique to monitor disease progression while a small molecule compound was administered as an antiprion therapeutic agent, in order to determine whether drug efficacy could be assessed more rapidly.

We monitored the efficacy of Compd B in two lines of prion-infected mice—wild-type (wt) and PrP-overexpressing Tg mice—both expressing the luciferase reporter gene under the control of the *Gfap* promoter. We report that monitoring GFAP induction

JPET Fast Forward. Published on August 21, 2013 as DOI: 10.1124/jpet.113.205799
This article has not been copyedited and formatted. The final version may differ from this version.

in vivo by measuring the luminescence signal enabled early detection of drug efficacy. To develop a more realistic *in vivo* model, we also performed intervention studies, administering compounds at different time points following prion infection (60–80 dpi). Disappointingly, we found that delayed treatment resulted in shorter extensions in survival.

MATERIALS AND METHODS

Ethics statement

All animal studies were approved by the Institutional Animal Care and Use Committee at the University of California San Francisco.

Cellular PrP^{Sc} reduction assay

Mouse N2a neuroblastoma cells (ATCC) were transfected with full-length mouse PrP and infected with the Rocky Mountain Laboratory (RML) strain of mouse-adapted scrapie prions, yielding ScN2a-cl3 cells (Ghaemmaghami et al., 2010). ScN2a-cl3 cells were maintained in tissue culture flasks (175 cm^2) containing 32 mL of filter-sterilized (0.2 µm) MEM with Earle's salts and L-glutamine, supplemented with 10% FBS, 250 µg/mL Geneticin, 50 I.U./mL penicillin, and 50 µg/mL streptomycin (supplemented MEM) in a humidified and CO_2-enriched (5%) environment at 37 °C. On day 1, the growth medium (supplemented MEM) was aspirated from the flasks, the cells washed twice with 10 mL of calcium- and magnesium-free Dulbecco's PBS, and then detached by addition of 3 mL of cell dissociation buffer after incubation at room temperature (RT)

JPET Fast Forward. Published on August 21, 2013 as DOI: 10.1124/jpet.113.205799
This article has not been copyedited and formatted. The final version may differ from this version.

for 5 min. The dissociation buffer was aspirated and the cells suspended in 10 mL of growth medium before counting using a Cellometer Auto T4 (Nexcelom Biosciences; Lawrence, MA). ScN2a-cl3 cells were seeded either into new, 175-cm^2 tissue culture flasks for continued cell culture (9×10^6 cells into 32 mL growth medium) or onto 96-well, tissue culture–treated, white polystyrene plates (Greiner Bio-One; Monroe, NC) for treatment with test compounds (40,000 cells/well in 100 μL of growth medium for dividing ScN2a cells; 150,000 cells/well in 80 μL of growth medium for stationary-phase ScN2a cells). Stationary-phase ScN2a-cl3 cells were allowed to adhere for 1 h at 37 °C before cell division arrest was induced by addition of 20 μL of 35 mM sodium butyrate in growth medium (7 mM final concentration) and the plates incubated for 24 h prior to compound addition. Dividing ScN2a-cl3 cells were allowed to adhere for 4 h at 37 °C before compound addition.

Test compounds (100 μL) were added to each well to attain a final concentration of 10 μM. Two positive controls were used: quinacrine and PAMAM-G4. Quinacrine (2 mM in 100% DMSO) was added, then diluted to a final concentration of 20 μM in growth medium (0.2% DMSO, final concentration). PAMAM-G4 was diluted from a 1% stock solution (in MeOH) to achieve a final concentration of 10 μg/mL. As a negative control, 0.2% DMSO in growth medium was used. Media was aspirated on day 5, and cells were washed with PBS (250 μL/well) and aspirated dry. The cells were lysed by addition of 20 μL of lysis buffer (10 mM Tris HCl, 150 mM NaCl, 0.5% sodium deoxycholate, 0.5% NP-40) containing 7.5 U/mL benzonase; plates were placed on a shaker at 37 °C for 1 h. Proteinase K [PK; 5 μL of 125 μg/mL in a Tris buffer (10 mM Tris HCl, 20 mM calcium chloride, 50% glycerol)] was added and incubated at 37 °C for

1 h, with shaking. PK digestion was stopped by addition of 5 µL of cold (4 °C) 20 mM PMSF in ethanol. After 10 min at RT, 10 µL of 5 M guanidine isothiocyanate was added at 37 °C for 1 h (with shaking) to denature the protein. The lysate in each well was diluted with 120 µL of PBS, and 150 µL from each well transferred to 96-well polystyrene ELISA plates previously coated with D18 antibody (5 µg/mL/well in 300 µL of acidified PBS overnight at RT in a humidified chamber (Safar et al., 2002)), the plates sealed, and incubated overnight at 5 °C. The next day, the plates were washed 3 times with TBST buffer (20 mM Tris HCl, 137 mM NaCl, 0.05% Tween-20, pH 7.5), the contents of each well aspirated completely. Then 100 µL of a 1:1000 dilution of HRP-conjugated D13 antibody was added and incubated at 37 °C for 1 h. The plates were washed 4 times with TBST buffer, the contents aspirated completely, and 100 µL of ABTS peroxidase substrate added to each well. After 15 min of development at RT, the enzymatic reaction was stopped by addition of 100 µL of ABTS stop solution and the plates immediately loaded onto a SpectraMax M5 plate reader (Molecular Devices; Sunnyvale, CA) for measurement of absorbance at 405 nm.

For cell viability assays, mouse N2a-cl3 cells were seeded into 96-well, black polystyrene plates (Greiner) and treated with compound as described above for the ELISA plates. After 5 days, the growth media was aspirated, the plates washed once with PBS (250 µL/well), and the plates aspirated dry. Calcein-AM (100 µL/well, 5 µg/mL solution in calcium- and magnesium-free PBS) was added, and the plates were incubated at 37 °C for 45 min. Fluorescent emission intensity was quantified using a Spectramax M5 plate reader, excitation/emission spectra of 485 nm/530 nm.

JPET Fast Forward. Published on August 21, 2013 as DOI: 10.1124/jpet.113.205799
This article has not been copyedited and formatted. The final version may differ from this version.

Computational methods

The Compd B structure was prepared and minimized in the Ligprep module of Schrödinger Software Suite 2010, after which it was subjected to geometry optimization in Jaguar (version 7.8, Schrödinger, LLC, New York, NY) using Density Functional Theory (DFT) (Hohenberg and Kohn, 1964; Kohn and Sham, 1965) with B3LYP functional and 6-31G** basis set. The DIIS convergence scheme and default convergence criteria were used: maximum iteration number of 48 and energy change of 5×10^{-5} hartrees.

Pharmacophore modeling was performed using Phase (version 3.2, Schrödinger, LLC, New York, NY). The ligands were prepared in Ligprep, where all stereoisomers and ionized species at pH 7 were generated and minimized. Next, conformers for each molecule were generated using mixed MCMM/LMOD method (Chang et al., 1989; Kolossváry and Guida, 1999) and OPLS 2005 force field (Jorgensen and Tirado-Rives, 1988; Kaminski et al., 2001). Parameters used in this step included a maximum of 1000 conformers per molecule, rapid sampling, and 100 minimization steps. RMSD cutoff of 1.0 Å was used to eliminate redundant conformers.

Chemistry of Compd B and analogs

One batch of Compd B was a generous gift from Professor Katsumi Doh-ura. The second batch was synthesized by ChemPartner (Shanghai, China). Amide Compd B isosteres that were not commercially available were synthesized using 2-(1H-7-azabenzotriazol-1-yl)-1,1,3,3-tetramethyluronium hexafluorophosphate (HATU)–assisted amide coupling reactions between an aryl carboxylic acid and 4-(2-

JPET Fast Forward. Published on August 21, 2013 as DOI: 10.1124/jpet.113.205799
This article has not been copyedited and formatted. The final version may differ from this version.

alkyl/cyclopropyloxazol-5-yl)anilines. The synthesis and characterization of these compounds are detailed in the *Supporting Information*.

Mice

FVB and CD-1 mice were purchased from Charles River (Hollister, CA). All Tg mice were on the FVB genetic background and bred at the Hunter's Point animal facility at UCSF. Tg(MHu2M,M111V,M165V,E167Q)1014/*Prnp*$^{0/0}$ mice were described previously (Giles et al., 2010). Tg(*Gfap*-luc) mice expressing the firefly luciferase reporter driven by a 12-kb fragment of the murine *Gfap* promoter (Zhu et al., 2004) were a gift from Caliper Life Sciences, from which a homozygous line was generated (Stöhr et al., 2012). Tg(MoPrP:*Gfap*-luc)4053 mice were obtained by crossing Tg mice overexpressing full-length MoPrP (Tg(MoPrP)4053 mice (Carlson et al., 1994; Telling et al., 1996)) with homozygous Tg(*Gfap*-luc) animals. Mice were housed with free access to food and water, and maintained on alternating 12-h light/dark cycles.

Pharmacokinetic studies

Single-dose pharmacokinetic studies were performed by oral gavage, with a compound concentration of 10 mg/kg in 200 µl of a formulation containing 20% propylene glycol, 5% labrosol, 5% ethanol, and 70% polyethylene glycol 400 (PEG400). At specified timepoints after dosing (0.5, 2, 4, and 6 h), mice were euthanized by CO_2, brain and plasma samples were collected and stored at -80 °C until analysis.

For quantification of Compd B and analogs, samples were injected onto a BDS Hypersil C8 column maintained at RT. The amount of acetonitrile (ACN) in the gradient was increased from 25% ACN to 95% ACN over 2.0 min, held for 1.0 min, and then re-

JPET Fast Forward. Published on August 21, 2013 as DOI: 10.1124/jpet.113.205799
This article has not been copyedited and formatted. The final version may differ from this version.

equilibrated to 25% ACN over 1.4 min. Data acquisition used MRM in the positive-ion mode, and the transitions monitored were m/z 265 → 160 for Compd B and m/z 321 → 253 for internal standard.

Microsomal incubations were performed with pooled female CD-1 mouse and human microsomes, obtained from BD Biosciences (San Jose, CA). Stock solutions (0.5 mM) of each compound prepared in DMSO were diluted 500-fold into 1 mL of microsomal incubation mixture (100 mM phosphate buffer, pH 7.4) and NADPH regenerating system (BD Biosciences), to yield a final concentration of 1 µM. This was preincubated at 37 °C for 5 min in an Eppendorf Thermo mixer, and the reaction initiated by addition of 0.5 mg (25 µl of a 20 mg/mL solution) of liver microsomes. Aliquots (50 µl) were withdrawn at 0, 5, 15, 30, and 60 min and added to 100 µl of ACN containing internal standard. These were then centrifuged at ~12,000 $\times$ *g* for 10 min. The supernatants were analyzed by LC/MS/MS. Duplicate incubations were run for each timepoint. The percentage of solute remaining at the end of the incubation was used to calculate the *in vitro* half-life ($t_{1/2}$), using $t_{1/2}$ = -0.693/k, where (-k) is the slope of the linear regression line from the plot of log percent remaining versus incubation time.

Mouse inoculation

Weaned mice (~8 weeks old) were inoculated intracerebrally with 30 µL of 1% brain homogenate either from mice infected with the RML prion strain or from a sCJD (type MM1) patient, diluted in filtered PBS containing 5% (wt/vol) bovine albumin Fraction V, using a 1-ml syringe and 27-gauge needle. Inoculated mice were examined every day,

JPET Fast Forward. Published on August 21, 2013 as DOI: 10.1124/jpet.113.205799
This article has not been copyedited and formatted. The final version may differ from this version.

and prion disease was diagnosed based on standard diagnostic criteria every 2–3 days (Carlson et al., 1988; Scott et al., 1993).

Long-term dosing of compounds

All calculations were based on typical wt FVB mouse weight of 25 g and liquid diet consumption of 20 ml per day. In practice, both mouse weight and food consumption increased over the duration of the study.

Rodent liquid diet was prepared by mixing 900 g of powdered diet (Bio Serv, product no. F1256SP), 50 g chocolate powder (Bio Serv, product no. 7345), and 4 L of water in a large stainless steel blender. For studies with Compd B, 2200 mg of compound was added to 200 mL of 100% PEG400. To ensure dissolution, vortexing and sonicating were applied. The solution was stored at -4 °C until use, then diluted 1:80 into the previously prepared rodent liquid diet, to make final dosing concentrations of 110 mg/kg/day with 1.25% PEG400. For untreated mice, pure PEG400 was diluted 1:80 into the previously prepared rodent liquid diet. The amount of food was served based on the number of animals in each cage and was replaced by new batches every two to three days.

Bioluminescence imaging

Mice were imaged weekly using an IVIS imaging system (Caliper Life Sciences). For each image, mice were intraperitoneally injected with 50 µL of 30 mg/mL D-luciferin potassium salt solution (Gold Biotechnology) in calcium- and magnesium-free PBS (Invitrogen). They were then anesthetized by an isoflurane-oxygen gas mix, and after 10 min, imaged for 60 s. Black construction paper cutouts were used as ear covers to

JPET Fast Forward. Published on August 21, 2013 as DOI: 10.1124/jpet.113.205799
This article has not been copyedited and formatted. The final version may differ from this version.

minimize noise signals from the ears. Bioluminescence values were quantified from Living Image 3.0 software (Caliper Life Sciences). Bioluminescence imaging (BLI) was initiated at 4–6 weeks postinoculation and continued weekly until animals were euthanized. For BLI curves, mean values were calculated from the same group of mice ($n \geq 3$) at each timepoint.

PrP^{Sc} detection by immunoblot

Twenty percent (wt/vol) brain homogenates were prepared from individual animals in calcium- and magnesium-free PBS, by 3 cycles of 60 s bead beating at 6500 rpm, placing tubes on ice between cycles, with a tissue homogenizer (Precellys). Protein concentrations were normalized using the bicinchoninic acid assay, and 750-µg aliquots were diluted to 1 ml with lysis buffer (10 mM Tris, pH 8.0; 150 mM NaCl; 0.5 % deoxycholic acid; 0.5% NP40). Digestion was performed by addition of 20 µg PK, incubated at 37 °C with shaking for 1 h. To stop the digestion, phenylmethylsulfonyl fluoride was added to a final concentration of 1 mM. Following ultracentrifugation at 100,000 $\times$ *g* at 4 °C, the supernatant was discarded and pellets were dissolved in 80 µl Nupage sample buffer, boiled, then run on a 4–12% Tris-glycine SDS gel (Invitrogen). The gel was transferred to a PVDF membrane using an iBlot (Invitrogen) and the membrane was blocked with 5% milk for 1 h at RT. The membranes were subsequently incubated overnight with human-mouse P Fab conjugated to horseradish peroxidase (HRP) and washed 3 times with TBST for 15 min before developing with the enhanced chemiluminescent reagent. Immunoblotting of CJD samples was performed as previously described (Giles et al., 2010).

JPET Fast Forward. Published on August 21, 2013 as DOI: 10.1124/jpet.113.205799
This article has not been copyedited and formatted. The final version may differ from this version.

Conformational-stability assay

Twenty microliters of 10% (wt/vol) brain homogenates were incubated with GdnHCl, in 0.5 M increments between 0 and 4 M, at 22 °C for 2 h. The samples were subsequently diluted with lysis buffer to a final concentration of 0.4 M of GdnHCl. Digestion and immunoblotting was performed as described above. Immunoblot gels were scanned and the densities of PrP^{Sc} bands were measured by ImageJ. The denaturation curves were generated based on band densities. The concentration at which 50% of PrP^{Sc} in the sample was denatured ($GdnHCl_{1/2}$) was then determined in Prism 6 (GraphPad Software, Inc., La Jolla, CA).

Statistical analysis

Statistical significance of differences observed between Compd B–treated and control samples from the conformational-stability assay was determined by using the Student's *t* test. The minimal level of significance was $P < 0.05$.

Pathology

After mice were euthanized, their right half-brains were fixed in 10% formalin for a minimum of 3 d. Fixed brains were processed and embedded in paraffin, and 8-µm sections were cut from four representative brain regions: cortex, cerebellum, hippocampus, and thalamus. Slides were deparaffinized and endogenous peroxidases blocked with 3% H_2O_2 in methanol for 30 min. The slides were washed 3 times for 5 min using PBS with 0.2% Tween 20 (PBST) with 3 buffer changes. Immunohistochemistry for PrP required antigen retrieval by hydrolytic autoclaving (1 mM citrate buffer, pH 6 at 121 °C for 10 min). Nonspecific antibody binding was blocked with 10% normal goat

JPET Fast Forward. Published on August 21, 2013 as DOI: 10.1124/jpet.113.205799
This article has not been copyedited and formatted. The final version may differ from this version.

serum (NGS) in PBST for 30 min. Slides were then incubated with the primary antibody: rabbit polyclonal anti-GFAP antibody (Dako) at 1:500 dilution, or the R2 monoclonal anti-PrP antibody (Williamson et al., 1998) at 5 µg/ml, in PBST at RT overnight. After washing, the sections were incubated with the appropriate biotinylated goat secondary antibody (Vector Labs, Burlingame, CA) at 1:100 in PBST with 10% NGS for 30 min at RT. After additional washing, the ABC kit (Vector) was used per the manufacturer's instructions. Sections were washed and developed with the DAB kit (Vector) for 1 min and washed again. Tween 20 was not present in the third wash. The sections were counterstained for 10 s in hematoxylin (Fisher), taken through graded alcohols to xylene, and coverslipped using Permount (Fisher). Images were taken at 20× and 40× magnifications using the SpotFlex camera and program on a Leica DM-IRB microscope.

RESULTS

Cellular PrP^{Sc} reduction by Compd B

The concentration-effect relationship of two independent batches of Compd B were determined in a five-day PrP^{Sc} reduction assay using ScN2a-cl3 cells, which overexpress PrP (**Figure 1**). Compd B, provided by Dr. Doh-Ura, almost entirely eliminated protease-resistant PrP^{Sc} with an EC_{50} of 0.31 ± 0.14 µM (*n*=4; **Figure 1A**). This value is different from the original potency of 60 pM reported in ScN2a cells, but similar to results using two clones of RML-infected N2a-58 cells, which also overexpress PrP (EC_{50} = 0.32 µM in N002, and EC_{50} = 0.3 µM in Ch2) (Kawasaki et al., 2007). Differences in potency might be caused by the heterogeneity of N2a subclones

JPET Fast Forward. Published on August 21, 2013 as DOI: 10.1124/jpet.113.205799
This article has not been copyedited and formatted. The final version may differ from this version.

(Mahal et al., 2007), or by the overexpression of PrP in the ScN2a-cl3 cells and N2a-58 cells relative to the wild-type expression of PrP in ScN2a cells. A second batch of Compd B, synthesized commercially at 100-g scale, had an EC_{50} of 0.76 ± 0.01 μM (*n*=3; **Figure 1B**) and was used for all subsequent studies.

Pharmacokinetic liabilities of Compd B

Despite the low EC_{50} values of Compd B in cell culture, and the promising efficacy indicated by the large extension in survival of treated mice (Kawasaki et al., 2007), further development of this compound into a drug candidate is unlikely, in large part due to the potential liability associated with the hydrazone functionality. This is a known toxicophore that undergoes Schiff base hydrolysis under physiologic conditions and releases aryl hydrazine, a toxic metabolite and carcinogen (Powell and Gannett, 2002). Aryl hydrazine is known to form DNA adducts, act as a DNA-cleaving agent (Hwu et al., 2004), and cause hemolytic anemia (Shalev et al., 1981). Thus, we sought new Compd B analogs that lack the liability associated with the undesirable hydrazone moiety yet maintain *in vivo* antiprion properties.

Pharmacophore model

New Compd B analogs were developed using a pharmacophore model built based on novel and diverse antiprion lead compounds discovered by high-throughput screening of RML-infected ScN2a-cl3 cells. Preliminary structure-activity relationship analysis of these leads suggested that a coplanar conjugated aromatic core structure is required for antiprion activity (Silber et al., manuscript in preparation). Lead compounds with a coplanar core structure were found to possess good antiprion potency (EC_{50} < 1 μM)

JPET Fast Forward. Published on August 21, 2013 as DOI: 10.1124/jpet.113.205799
This article has not been copyedited and formatted. The final version may differ from this version.

whereas compounds with a nonplanar scaffold structure showed only moderate activity (EC_{50} > 1 μM). To build the pharmacophore model of PrP^{Sc} leads, we started with 440 compounds for which EC_{50} values of PrP^{Sc} reduction were determined in ScN2a-cl3 cells. We defined actives as those with EC_{50} < 10 μM (*n* = 274) and inactives as EC_{50} ≥10 μM (*n* = 166). The pharmacophore modeling was performed using Phase (version 3.2; Schrödinger, Inc.) (Dixon et al., 2006). Pharmacophore sites were assigned using a set of features defined in Phase as hydrogen-bond acceptor (HBA), hydrogen-bond donor (HBD), hydrophobic group, negatively charged group, positively charged group, and aromatic ring. Common pharmacophore hypotheses were identified using tree-based partitioning techniques and were consequently scored and ranked. Final pharmacophore analysis indicated that more than half of the active compounds, *n* = 150, fell within a four-site pharmacophore (**Figure 2A**), with one HBD (blue), one HBA (red), and two aromatic sites (rings). The HBD and HDA are arranged into a linker that connects the two aromatic sites.

Computational analysis of the Compd B structure suggests that the molecule adopts a near coplanar conformation similar to the pharmacophore model (**Figure 2B**). However, the HBA atom of Compd B, unlike in the model, links directly to the HBD atom and is displaced from the optimal location described by the model. Thus, for new Compd B analogs, we decided to replace the 3-atom linker with a 2-atom linker, such as an amide bond that contains a HBA (C=O) and HBD (NH), fitting well with the pharmacophore model.

JPET Fast Forward. Published on August 21, 2013 as DOI: 10.1124/jpet.113.205799
This article has not been copyedited and formatted. The final version may differ from this version.

Analogs of Compd B

To test the hypothesis we developed from the pharmacophore model above, we first synthesized a Compd B analog, replacing the hydrazone linker by an amide (**1**). However, this compound was completely inactive in ScN2a-cl3 cells (**Table 1**). Replacing the pyridyl with a phenyl group restored the antiprion activity: the unsubstituted benzamide **2** had an EC_{50} of 0.64 ± 0.07 μM. Addition of an electron-donating group resulted in greatly improved potency: the 4-methoxy analog **3** had an EC_{50} of 0.12 ± 0.01 μM. Several other benzamide analogs (**4**–**6**) were tested; 4-Cl (**4**) and 3-MeO,4-Me (**5**) had similar potency to **3**, while the 2,4-diF analog **6** was approximately 3-fold less potent than **3**.

Encouraged by the potency of **3**–**5**, we dosed these compounds in mice to evaluate their pharmacokinetic profiles and determined *in vitro* metabolic stability in human and mouse hepatic microsomes (**Table 2**). Compound **3** displayed poor pharmacokinetic characteristics, relative to Compd B, with low plasma and brain exposures likely caused by its low metabolic stability in mouse hepatic microsomes ($t_{1/2}$ = 7 min). Compounds **4** and **6** showed slightly improved metabolic stability as well as brain and plasma exposures compared to **3**. Compound **5** displayed better metabolic stability ($t_{1/2}$= 20 min) and thus better brain and plasma exposures.

To improve the metabolic stability and pharmacokinetic profiles of these analogs, we sought to introduce a methyl or cyclopropyl group at the 2-position of the oxazole ring to block any oxidation at this site. A total of 12 analogs were purchased or synthesized (**7**–**18**). Substitution at the *para*-position of the phenyl ring is favored for

JPET Fast Forward. Published on August 21, 2013 as DOI: 10.1124/jpet.113.205799
This article has not been copyedited and formatted. The final version may differ from this version.

antiprion potency, with analogs **8**, **12**, **14** and **15** displaying the best potency (EC_{50} = 0.06–0.19 μM; **Table 1**). In the case of fluoro-substituted benzamides, **12** (4-F) was up to 7-fold more potent than its positional isomers **10** (2-F), **11** (3-F), and **13** (2,4-diF). Cyano analog **16** and 3-Me **18** had EC_{50} values of ~0.35 μM. However, two *para*-substituted cyano analogs (**7** and **17**) displayed only moderate antiprion potency (EC_{50} of ~0.5 μM). Analog **9**, with 2-$NCCH_2S$, was inactive in our assays.

When tested *in vitro* for metabolic stability and *in vivo* for brain and plasma exposure, many of these methyl- or cyclopropyl-substituted oxazole analogs showed improved pharmacokinetic profiles (**Table 2**). Fluoro analogs **10** and **11**, cyano analogs **16** and **17**, and 3-Me **18** had $t_{1/2}$ longer than 20 min in mouse hepatic microsomes as well as improved brain and plasma exposures compared to Compd B. All four fluoro analogs (**10**–**13**) showed higher brain exposures (C_{max} and AUC) compared to Compd B. Electron-rich analog **15** (4-MeOEtO) had poor stability in mouse hepatic microsomal preparations ($t_{1/2}$ = 11 min). Interestingly, compound **14** (4-Cl), with an electron-withdrawn group, also showed poor microsomal stability ($t_{1/2}$ = 7 min). Not surprisingly, both **14** (4-Cl) and **15** (4-MeOEtO) displayed poor plasma and brain exposures in mouse pharmacokinetic studies. More importantly, the brain C_{max} values for several analogs (**10**, **12**, **13** and **16**) were at least 10-fold their corresponding EC_{50} values.

Overall, six analogs (**10**, **12**, **13** and **16**–**18**) showed improved antiprion potency (**Table 1**) and better pharmacokinetic results (**Table 2**) than Compd B, suggesting they may be more suitable candidates as antiprion therapeutics.

JPET Fast Forward. Published on August 21, 2013 as DOI: 10.1124/jpet.113.205799
This article has not been copyedited and formatted. The final version may differ from this version.

Long-term dosing of Compd B for efficacy studies

While designing more potent and less toxic compounds as therapeutics for prion disease, we pursued finding a more efficient technique to measure the efficacy of candidate molecules in mouse models, with the hope that a well-validated animal system will be in place when new candidate drugs are identified. Because Compd B is the only small molecule demonstrated to substantially extend survival in prion-infected mice, it was used as a positive indicator for the purpose of setting up and evaluating our animal testing procedure.

From previous studies, dosing at 100 mg/kg/day of Compd B to FVB mice for 3 days in a liquid diet resulted in brain concentrations of ~10 μM, 25 times higher than the EC_{50} value of 0.4 μM in ScN2a-cl3 cells. However, doses of 150 mg/kg/day for 8 days resulted in 2 of 4 animals dying (Silber et al., 2013). Therefore, we selected a dose between the two, of 110 mg/kg/day, to be used in future long-term *in vivo* dosing studies. To apply continuous dosing, Compd B was mixed into a liquid diet along with 1.25% of PEG400 as an excipient to enable the dissolution of the compound. In preliminary studies, we observed male mice had a high mortality rate after 2–3 months when PEG400 was included in their food. From whole body pathologic examination of two individual cases, both animals showed a distended urinary bladder that contained globular substance lining the lumen. It is likely that PEG400 was excreted into the urine and precipitated in the bladder, resulting in diminished bladder function and distension. In comparison, female mice dosed for up to 280 days showed no signs of intolerance to PEG400. As a result, all further experiments were performed in female mice only.

To determine concentrations of Compd B in the brain upon longer-term dosing, we collected brains from mice dosed at 110 mg/kg/day for 7, 14, 21 and 28 days (**Supporting Table 1**). Unexpectedly, there was no correlation between duration of dosing and the concentration of Compd B in the brain. Occasionally, values above 10 µM were observed, but the majority of mice had very low levels in the brain. This lack of correlation likely reflects the rapid metabolic half-life of Compd B (15 min), and the variability between when mice last ate (and thus dosed) and when they were euthanized for analysis. These observations imply that brain concentrations likely vary widely over the course of each day.

Compd B prolonged survival in Tg(*Gfap*-luc) mice

Despite the lack of sustained high levels of Compd B in the brain, Compd B doses of 300 mg/kg/day were reported to double survival of RML-infected Tga20 mice that overexpress MoPrP (Kawasaki et al., 2007). Compd B increased the incubation time 69 ± 6 to 154 ± 20 days. Using mice that did not overexpress wt MoPrP, we administered orally Compd B at 110 mg/kg/day; the drug was diluted in 1.25% PEG400 in a chocolate liquid diet.

To determine whether extended survival could be predicted by BLI, FVB mice expressing a transgene encoding luciferase under control of the *Gfap* promoter were inoculated intracerebrally with RML prions. Compd B treatment was initiated one day after inoculation with RML prions and continued until mice showed signs of neurologic dysfunction, at which time they were euthanized. Untreated prion-infected Tg(*Gfap*-luc) mice were fed 1.25% PEG400 dissolved in the chocolate liquid diet. The

JPET Fast Forward. Published on August 21, 2013 as DOI: 10.1124/jpet.113.205799
This article has not been copyedited and formatted. The final version may differ from this version.

bioluminescence signal measured from untreated, RML-infected Tg(*Gfap*-luc) mice showed a sustained increase beginning at ~55 dpi, which is consistent with previous findings (Tamgüney et al., 2009); these mice showed signs of neurologic dysfunction at 108 ± 1 dpi (*n*=8; **Figure 3A and C**). In contrast, the BLI signal in Tg(*Gfap*-luc) mice treated with Compd B remained unchanged for ~200 dpi, providing an early, non-invasive indication that treatment was likely to be efficacious (**Figure 3C**). The average BLI signal increased about 6-fold beginning at ~200 dpi and plateaued for 30–40 days prior to the appearance of signs of neurologic dysfunction. The mean incubation time for the Compd B–treated group was 219 ± 21 days (*n*=10) (**Table 3**), indicating that Compd B prolonged survival of RML-infected mice by more than 100 d and that its efficacy could be monitored by BLI.

Compd B prolonged survival in Tg mice overexpressing MoPrP

To determine whether BLI could also be predictive of Compd B efficacy in mice overexpressing MoPrP, we used mice expressing two transgenes: MoPrP and *Gfap*-luc. These bigenic mice were designated Tg(MoPrP:*Gfap*-luc)4053 mice, which express full-length MoPrP at a level ~4-fold higher than that of endogenous PrP. The Tg(MoPrP:*Gfap*-luc)4053 mice have an incubation time of ~50 days after intracerebral inoculation with RML prions and showed a sustained increase in bioluminescence beginning ~30 dpi (**Figure 3B and D**). In these bigenic mice, Compd B treatment extended the time interval from inoculation to an increase in the BLI signal from ~30 to ~120 dpi and prolonged the time at which signs of neurologic dysfunction were detected from 52 ± 2 d (*n*=15) to 143 ± 7 d (*n*=12). Notably, Compd B extended both the time

JPET Fast Forward. Published on August 21, 2013 as DOI: 10.1124/jpet.113.205799
This article has not been copyedited and formatted. The final version may differ from this version.

from inoculation to an increase in the BLI signal and to the manifestation of neurologic dysfunction by ~90 days (**Figure 3B and D, Table 3**).

Immunoblotting of brain samples from Tg(*Gfap*-luc) mice treated with Compd B showed protease-resistant PrP^{Sc} bands (**Figure 4A**). Overall, mice developing clinical signs at earlier time points showed less PrP^{Sc} in their brains compared to mice at later time points, but some interanimal variabilities were observed.

To determine if Compd B altered the prion strain characteristics, we measured the conformational stability of RML prions in the brains of Compd B–treated Tg(*Gfap*-luc) mice. GdnHCl denaturation curves for PrP^{Sc} were determined using homogenates prepared from untreated and Compd B–treated Tg(*Gfap*-luc) mice (**Figure 4B**). PrP^{Sc} in untreated mice exhibited a $GdnHCl_{1/2}$ value of 1.4 ± 0.2 M (n=6) while the treated mice showed a $GdnHCl_{1/2}$ value of 1.8 ± 0.3 M (n=5). This analysis demonstrated that the PrP^{Sc} in treated mice was significantly more stable than that in the untreated mouse brains (p = 0.014). These findings argue that a conformational change occurred in PrP^{Sc} as a result of exposure to Compd B.

Consistent with a difference in conformational stability, neuropathologic differences were also observed between untreated and Compd B–treated Tg(*Gfap*-luc) mice (**Figure 4C–H**). Untreated mice showed uniform deposition of PrP^{Sc} in all regions of the brain and brainstem (**Figure 4D**). In contrast, the treated mice showed a patchy distribution of PrP^{Sc}, which was most evident in the thalamus and brainstem, but largely absent from the hippocampus and cerebral cortex, which was consistent even for mice that had high levels of PK-resistant PrP (**Figure 4G**). GFAP staining showed moderately

JPET Fast Forward. Published on August 21, 2013 as DOI: 10.1124/jpet.113.205799
This article has not been copyedited and formatted. The final version may differ from this version.

intense astrocytic gliosis in all brain areas of untreated mice (**Figure 4E**) but minimal astrocytic gliosis was found in 4 of 6 Compd B–treated mice (**Figure 4H**). In addition, H&E staining revealed only a few vacuoles in the hippocampus and no nerve cell loss in both untreated and treated mice (**Figure 4C and F**).

Immunoblotting of brain samples from Tg(MoPrP:*Gfap*-luc)4053 mice treated with Compd B showed protease-resistant PrP^{Sc} bands (**Figure 5A**). As with Tg(*Gfap*-luc) mice, animals developing signs of neurological dysfunction at earlier time points harbored less protease-resistant PrP^{Sc} in their brains compared to ill mice at later time points.

To determine if Compd B altered the prion strain characteristics in Tg(MoPrP:*Gfap*-luc)4053 mice, we measured the conformational stability of RML prions in the brains of these bigenic mice. GdnHCl denaturation curves for PrP^{Sc} were determined using homogenates prepared from untreated and Compd B–treated mice (**Figure 5B**). PrP^{Sc} in untreated Tg(MoPrP:*Gfap*-luc)4053 mice exhibited a $GdnHCl_{1/2}$ value of 1.4 ± 0.3 M (n=6) while that in the treated mice possessed a $GdnHCl_{1/2}$ value of 1.7 ± 0.2 M (n = 6). In contrast to the increase in conformational stability of PrP^{Sc} attributed to Compd B in Tg(*Gfap*-luc) mice (**Figure 4B**), the increased stability of PrP^{Sc} in Tg(MoPrP:*Gfap*-luc)4053 mice was not statistically significant (p = 0.079).

Like the differences in neuropathology with untreated and Compd B–treated Tg(*Gfap*-luc) mice (**Figure 4C–H**), substantial differences were found in the neuropathology of untreated and Compd B–treated Tg(MoPrP:*Gfap*-luc)4053 mice (**Figure 5C–H**). Untreated Tg(MoPrP:*Gfap*-luc)4053 mice showed substantially more intense deposition of PrP^{Sc} (**Figure 5D**) compared to treated mice, which had broader

JPET Fast Forward. Published on August 21, 2013 as DOI: 10.1124/jpet.113.205799
This article has not been copyedited and formatted. The final version may differ from this version.

distribution of patchy PrP^{Sc} clusters, including a greater area of accumulation in the thalamus and patchy accumulation in the hippocampus, cerebral cortex, and brainstem (**Figure 5G**). GFAP staining revealed a moderate astrocytic gliosis in all regions and intense astrocytic gliosis in the hippocampus of untreated mice (**Figure 5E**). In contrast, the treated group showed a moderate degree of astrocytic gliosis in areas where patchy deposits of PrP^{Sc} appeared (**Figure 5H**). Similar to Tg(*Gfap*-luc) mice, H&E staining of Tg(MoPrP:*Gfap*-luc)4053 brains did not show any pathology, with only a few vacuoles seen in the hippocampus and no nerve cell loss (**Figure 5C and F**).

Compd B was ineffective against CJD prions

While the foregoing results with Tg mice inoculated with RML prions were encouraging, we asked if Compd B could extend the lives of Tg mice inoculated with CJD prions. To investigate this possibility, we chose Tg(MHu2M,M111V,M165V,E167Q)1014/$Prnp^{0/0}$ mice, which have abbreviated incubation times for human CJD prions (Giles et al., 2010). The Tg1014 mice express a chimeric mouse/human PrP transgene and develop signs of neurologic dysfunction in ~80 days after inoculation with the MM1 subtype of CJD prions. After we administered 110 mg/kg/day of Compd B to Tg1014 mice infected with CJD(MM1) prions beginning at 1 dpi, we observed no extension in survival of the Tg1014 mice. Those Tg1014 mice receiving Compd B displayed signs of neurologic dysfunction at 78 ± 1 days compared to 80 ± 1 days for the untreated controls (**Figure 6A**). Analysis of brains, both biochemically and neuropathologically, also failed to show any differences. By immunoblotting, levels of PrP^{Sc} in the brains of treated mice were indistinguishable from the untreated controls (**Figure 6B**). Neuropathologic analysis showed that both untreated (**Figure 6C–E**) and treated (**Figure 6F–H**) Tg1014 mice

JPET Fast Forward. Published on August 21, 2013 as DOI: 10.1124/jpet.113.205799
This article has not been copyedited and formatted. The final version may differ from this version.

infected with CJD prions had widespread vacuolation, punctate PrP^{Sc} deposition, and strong astrocytic gliosis.

Delayed administration of Compd B

Tg(*Gfap*-luc) mice were treated with Compd B beginning 60 or 78 days after intracerebral inoculation with RML prions (**Figure 7, Table 3**). Compared to mice treated with Compd B beginning 1 dpi that had incubation periods of 219 dpi, those receiving Compd B beginning 60 dpi showed a reduced survival time of 182 dpi. A further reduction in survival time, to 163 dpi, was found when the Tg(*Gfap*-luc) mice were treated with Compd B beginning 78 dpi. These reductions in the effectiveness of Compd B are consistent with results from an earlier study (Kawasaki et al., 2007).

Immediately after initiation of Compd B therapy at either 60 or 78 dpi, we found that the BLI signal increased rapidly to very high levels (**Figure 7C and D**). After 30 to 50 days, the bioluminescence level fell to ~2×10^6 photons/s and remained there until approximately 150 dpi. Over the next 50 days, the BLI signal remained above ~8×10^6 photons/s as the mice developed signs of neurologic dysfunction. Of note, three mice in the 60-dpi group were found dead in the cage, and one mouse in the 78-dpi group showed clinical signs of neurologic dysfunction, including ataxia, circling, weight loss, and dull hair coat. Those mice were excluded in the calculations of mean survival.

JPET Fast Forward. Published on August 21, 2013 as DOI: 10.1124/jpet.113.205799
This article has not been copyedited and formatted. The final version may differ from this version.

DISCUSSION

Growing evidence argues that many neurodegenerative disorders, including Alzheimer's and Parkinson's diseases as well as the tauopathies and ALS, result from a particular protein becoming a prion (Meyer-Luehmann et al., 2006; Clavaguera et al., 2009; Frost et al., 2009; Grad et al., 2011; Münch et al., 2011; Luk et al., 2012; Mougenot et al., 2012; Prusiner, 2012). The single major risk factor for all these diseases is age, and changing demographics imply that neurodegenerative diseases will become the major burden to healthcare systems in the coming decades. Developing effective therapeutics against neurodegenerative disease therefore represents an urgent unmet need.

While many compounds have been reported that are effective against cell models of prion disease, the only small molecule to substantially extend survival in prion-infected mice is Compd B (Kawasaki et al., 2007). However, this molecule is rapidly metabolized, which requires frequent, high doses to sustain sufficient concentrations in the brain to achieve therapeutic efficacy. Furthermore, Compd B suffers from a toxicophore in the form of a hydrazone. Based on analysis of diverse antiprion lead compounds, including Compd B, we developed a four-site pharmacophore model consisting of two aromatic rings separated by a two-atom linker containing a hydrogen bond donor and a hydrogen bond acceptor. We therefore developed Compd B analogs in which the hydrazone was replaced by an amide. The direct amide analog of Compd B (**1**), was inactive in ScN2a-cl3 cells; however, replacement of the pyridyl group with a phenyl group (**2**) restored antiprion activity. Based on this compound, we determined structure-activity relationships using selected

modifications to the phenyl and oxazole rings (**Table 1**). Blocking the oxidation of the oxazole moiety by introduction of an alkyl group, and introducing an electron-withdrawing group to the phenyl ring, increased potency and metabolic stability. Of the 18 novel compounds tested, four compounds (**10, 12, 13** and **16**) had maximal drug concentrations (C_{max}) in the brain that were 10-fold greater than their respective EC_{50} values. The efficacy of these compounds *in vivo* remains to be determined.

Compd B administered to prion-infected Tg mice prolonged survival but with some variability (**Figures 3 and 7**), which was also observed in immunoblots between individual animals treated with Compd B (**Figures 4 and 5**). This variability might be explained by the dosing administration. While dispensing Compd B in a liquid diet is convenient and enables continuous dosing in the long timescales required in mouse models of neurodegenerative disease, it might also result in wide fluctuations in drug concentrations in the brains of mice (**Supporting Table 1**). Mice feed at discrete intervals that are more frequent during the dark cycle; during the light cycle, gaps between feeding periods can be on the order of hours (Goulding et al., 2008). For a compound with $t_{1/2}$ of ~15 min, such as Compd B, tissue concentration can drop ~4000-fold in 3 h. Therefore, over the course of each day, treated mice are likely to have large variations in brain concentrations of Compd B, which may account for the disparities in survival extensions that we observed.

BLI has proved useful in monitoring neurodegeneration in various Tg mouse models (Keller et al., 2009; Tamgüney et al., 2009; Watts et al., 2011). Here we demonstrate that it can be used to predict drug efficacy before extension in survival is evident. When the BLI signal began to increase in untreated mice infected with the RML

JPET Fast Forward. Published on August 21, 2013 as DOI: 10.1124/jpet.113.205799
This article has not been copyedited and formatted. The final version may differ from this version.

prion strain, the signal remained unchanged in RML-infected mice given Compd B beginning at 1 dpi (**Figure 3**). BLI proved less useful when therapeutic intervention was initiated later (**Figure 7**) due to the abrupt increase in bioluminescence. The BLI signal is an indirect measure of gene expression, relying on the amount of luciferin substrate crossing the blood-brain barrier (BBB) and the appropriate cofactor availability for luciferase. One possible scenario as prion disease progresses is that the BBB may be more susceptible to disruption upon introduction of Compd B; this might explain the rapid increases in bioluminescence observed when dosing was started at 60 or 78 dpi.

Brains from RML-infected mice treated with Compd B occasionally showed lower levels of PrP^{Sc} than untreated mice, but in all cases there was no difference in the sizes or proportions of PK-resistant PrP glycoforms. However, conformational stability of PrP^{Sc}, as determined by GdnHCl denaturation, suggested a change in strain (Peretz et al., 2001), with Compd B–treated mice exhibiting higher $GdnHCl_{1/2}$ values (**Figures 4B and 5B**). Moreover, neuropathological analysis of brains from Compd B–treated mice differed substantially from untreated controls: even when treated and untreated mice showed similar levels of PrP^{Sc} by immunoblot, Compd B–treated mice showed sparse and patchy PrP by immunohistochemistry (**Figures 4G and 5G**). Treatment with drugs can result in the transformation of prion strains (Ghaemmaghami et al., 2009; Li et al., 2010; Ghaemmaghami et al., 2011). In these studies, Compd B may directly or indirectly interact with PrP^{Sc}, resulting in an alternative PrP^{Sc} conformation.

Our studies with Compd B treatment showed an extension in survival, but all infected mice eventually succumbed to disease. If prion strains represent ensembles of conformations, then Compd B treatment might be effective against the major strain

conformation but not against other conformations in the RML inocula. In an earlier study, Compd B showed a modest extension of the survival of mice inoculated with the mouse-passaged human prion strain Fukuoka-1 (Kawasaki et al., 2007). However, we observed no efficacy of Compd B against sCJD(MM1) prions inoculated into Tg1014 mice (**Figure 6**); sCJD(MM1) prions are most common human strain. These findings emphasize the need to perform drug efficacy studies on human prion strains (Giles et al., 2008) whenever possible.

Our findings with Compd B have important implications for the development of antiprion therapeutics. The new lead compounds developed here, and the application of BLI to drug efficacy studies, should advance efforts toward developing effective therapeutics for prion diseases.

ACKNOWLEDGMENTS

We thank Ms. Sumita Bhadwaj and Dr. Smita Patel for technical assistance, and the staff of the Hunter's Point animal facility. We also thank Dr. Katsumi Doh-ura for his generous gift of Compd B, Dr. Robert Wilhelm for helpful suggestions on the manuscript, Dr. Shenheng Guan and Mr. Shigenari Hayashi for technical assistance, and Ms. Hang Nguyen for expert editorial assistance.

AUTHOR CONTRIBUTIONS

Participated in research design: Lu, Giles, Geva, Prusiner.

Conducted experiments: Lu, Li, Rao, Dolghih, Gever, Geva, Elepano, Oehler, DeArmond.

Contributed new reagents or analytic tools: Bryant, Renslo, Silber.

Performed data analysis: Lu, Giles, Li, Rao, Jacobson, DeArmond, Prusiner.

Wrote or contributed to the writing of the manuscript: Lu, Giles, DeArmond, Prusiner.

REFERENCES

Aguzzi A, Sigurdson C and Heikenwaelder M (2008) Molecular mechanisms of prion pathogenesis. *Annu. Rev. Pathol.* **3**:11-40.

Carlson GA, Ebeling C, Yang S-L, Telling G, Torchia M, Groth D, Westaway D, DeArmond SJ and Prusiner SB (1994) Prion isolate specified allotypic interactions between the cellular and scrapie prion proteins in congenic and transgenic mice. *Proc. Natl. Acad. Sci. U.S.A.* **91**:5690-5694.

Carlson GA, Goodman PA, Lovett M, Taylor BA, Marshall ST, Peterson-Torchia M, Westaway D and Prusiner SB (1988) Genetics and polymorphism of the mouse prion gene complex: control of scrapie incubation time. *Mol. Cell. Biol.* **8**:5528-5540.

Chang G, Guida WC and Still WC (1989) An internal coordinate Monte Carlo method for searching conformational space. *J. Am. Chem. Soc.* **111**:4379–4386.

Clavaguera F, Bolmont T, Crowther RA, Abramowski D, Frank S, Probst A, Fraser G, Stalder AK, Beibel M, Staufenbiel M, Jucker M, Goedert M and Tolnay M (2009) Transmission and spreading of tauopathy in transgenic mouse brain. *Nat. Cell Biol.* **11**:909–913.

Dixon SL, Smondyrev AM, Knoll EH, Rao SN, Shaw DE and Friesner RA (2006) PHASE: a new engine for pharmacophore perception, 3D QSAR model development, and 3D database screening: 1. Methodology and preliminary results. *J. Comput. Aided Mol. Des.* **20**:647–671.

Frost B, Jacks RL and Diamond MI (2009) Propagation of tau misfolding from the outside to the inside of a cell. *J. Biol. Chem.* **284**:12845–12852.

Ghaemmaghami S, Ahn M, Lessard P, Giles K, Legname G, DeArmond SJ and Prusiner SB (2009) Continuous quinacrine treatment results in the formation of drug-resistant prions. *PLoS Pathog.* **5**:e1000673.

Ghaemmaghami S, Ullman J, Ahn M, St. Martin S and Prusiner SB (2010) Chemical induction of misfolded prion protein conformers in cell culture. *J. Biol. Chem.* **285**:10415–10423.

Ghaemmaghami S, Watts JC, Nguyen H-O, Hayashi S, DeArmond SJ and Prusiner SB (2011) Conformational transformation and selection of synthetic prion strains. *J. Mol. Biol.* **413**:527–542.

Giles K, Glidden DV, Beckwith R, Seoanes R, Peretz D, DeArmond SJ and Prusiner SB (2008) Resistance of bovine spongiform encephalopathy (BSE) prions to inactivation. *PLoS Pathog.* **4**:e1000206.

Giles K, Glidden DV, Patel S, Korth C, Groth D, Lemus A, DeArmond SJ and Prusiner SB (2010) Human prion strain selection in transgenic mice. *Ann. Neurol.* **68**:151–161.

Goulding EH, Schenk AK, Juneja P, MacKay AW, Wade JM and Tecott LH (2008) A robust automated system elucidates mouse home cage behavioral structure. *Proc. Natl. Acad. Sci. USA* **105**:20575–20582.

Grad LI, Guest WC, Yanai A, Pokrishevsky E, O'Neill MA, Gibbs E, Semenchenko V, Yousefi M, Wishart DS, Plotkin SS and Cashman NR (2011) Intermolecular transmission of superoxide dismutase 1 misfolding in living cells. *Proc. Natl. Acad. Sci. USA* **108**:16398–16403.

Hohenberg P and Kohn W (1964) Inhomogeneous electron gas. *Phys. Rev.* **136**:B864–B871.

Hwu JR, Lin CC, Chuang SH, King KY, Su TR and Tsay SC (2004) Aminyl and iminyl radicals from arylhydrazones in the photo-induced DNA cleavage. *Bioorg. Med. Chem.* **12**:2509–2515.

Jorgensen WL and Tirado-Rives J (1988) The OPLS potential functions for proteins. Energy minimizations for crystals of cyclic peptides and crambin. *J. Am. Chem. Soc.* **110**:1657–1666.

Kaminski GA, Friesner RA, Tirado-Rives J and Jorgensen WL (2001) Evaluation and reparametrization of the OPLS-AA force field for proteins via comparison with accurate quantum chemical calculations on peptides. *J. Phys. Chem. B* **105**:6474–6487.

Kawasaki Y, Kawagoe K, Chen CJ, Teruya K, Sakasegawa Y and Doh-ura K (2007) Orally administered amyloidophilic compound is effective in prolonging the incubation periods of animals cerebrally infected with prion diseases in a prion strain-dependent manner. *J. Virol.* **81**:12889-12898.

Keller AF, Gravel M and Kriz J (2009) Live imaging of amyotrophic lateral sclerosis pathogenesis: Disease onset is characterized by marked induction of GFAP in Schwann cells. *Glia* **57**:1130–1142.

Kohn W and Sham LJ (1965) Self-consistent equations including exchange and correlation effects. *Phys. Rev.* **140**:A1133–A1138.

Kolossváry I and Guida WC (1999) Low-mode conformational search elucidated: Application to $C_{39}H_{80}$ and flexible docking of 9-deazaguanine inhibitors into PNP. *J. Comput. Chem.* **20**:1671–1684.

Li J, Browning S, Mahal SP, Oelschlegel AM and Weissmann C (2010) Darwinian evolution of prions in cell culture. *Science* **327**:869–872.

Luk KC, Kehm VM, Zhang B, O'Brien P, Trojanowski JQ and Lee VMY (2012) Intracerebral inoculation of pathological α-synuclein initiates a rapidly progressive neurodegenerative α-synucleinopathy in mice. *J. Exp. Med.* **209**:975–986.

Mahal SP, Baker CA, Demczyk CA, Smith EW, Julius C and Weissmann C (2007) Prion strain discrimination in cell culture: the cell panel assay. *Proc. Natl. Acad. Sci. USA* **104**:20908–20913.

Meyer-Luehmann M, Coomaraswamy J, Bolmont T, Kaeser S, Schaefer C, Kilger E, Neuenschwander A, Abramowski D, Frey P, Jaton AL, Vigouret JM, Paganetti P, Walsh DM, Mathews PM, Ghiso J, Staufenbiel M, Walker LC and Jucker M (2006) Exogenous induction of cerebral beta-amyloidogenesis is governed by agent and host. *Science* **313**:1781-1784.

Mougenot A-L, Nicot S, Bencsik A, Morignat E, Verchère J, Lakhdar L, Legastelois S and Baron T (2012) Prion-like acceleration of a synucleinopathy in a transgenic mouse model. *Neurobiol. Aging* **33**:2225–2228.

Münch C, O'Brien J and Bertolotti A (2011) Prion-like propagation of mutant superoxide dismutase-1 misfolding in neuronal cells. *Proc. Natl. Acad. Sci. USA* **108**:3548–3553.

Peretz D, Scott M, Groth D, Williamson A, Burton D, Cohen FE and Prusiner SB (2001) Strain-specified relative conformational stability of the scrapie prion protein. *Protein Sci.* **10**:854-863.

Powell JH and Gannett PM (2002) Mechanisms of carcinogenicity of aryl hydrazines, aryl hydrazides, and arenediazonium ions. *J. Environ. Pathol. Toxicol. Oncol.* **21**:1–31.

Prusiner SB (1998) Prions. *Proc. Natl. Acad. Sci. U.S.A.* **95**:13363-13383.

Prusiner SB (2007) Prions, in *Fields Virology* (Knipe DM, Howley PM, Griffin DE, Lamb RA, Martin MA, Roizman B and Straus SE eds) pp 3059-3092, Lippincott Williams & Wilkins, Philadelphia.

Prusiner SB (2012) A unifying role for prions in neurodegenerative diseases. *Science* **336**:1511–1513.

Richt JA and Hall SM (2008) BSE case associated with prion protein gene mutation. *PLoS Pathog.* **4**:e1000156.

Safar JG, Scott M, Monaghan J, Deering C, Didorenko S, Vergara J, Ball H, Legname G, Leclerc E, Solforosi L, Serban H, Groth D, Burton DR, Prusiner SB and Williamson RA (2002) Measuring prions causing bovine spongiform encephalopathy or chronic wasting disease by immunoassays and transgenic mice. *Nat. Biotechnol.* **20**:1147-1150.

Scott M, Groth D, Foster D, Torchia M, Yang S-L, DeArmond SJ and Prusiner SB (1993) Propagation of prions with artificial properties in transgenic mice expressing chimeric PrP genes. *Cell* **73**:979-988.

Shalev O, Leida MN, Hebbel RP, Jacob HS and Eaton JW (1981) Abnormal erythrocyte calcium homeostasis in oxidant-induced hemolytic disease. *Blood* **58**:1232–1235.

Silber BM, Rao S, Fife KL, Gallardo-Godoy A, Renslo AR, Dalvie DK, Giles K, Freyman Y, Elepano M, Gever JR, Li Z, Jacobson MP, Huang Y, Benet LZ and Prusiner SB (2013) Pharmacokinetics and metabolism of 2-aminothiazoles with antiprion activity in mice. *Pharm. Res.* **30**:932–950.

Sim VL (2012) Prion disease: chemotherapeutic strategies. *Infect. Disord. Drug Targets* **12**:144–160.

Stöhr J, Watts JC, Mensinger ZL, Oehler A, Grillo SK, DeArmond SJ, Prusiner SB and Giles K (2012) Purified and synthetic Alzheimer's amyloid beta (Aβ) prions. *Proc. Natl. Acad. Sci. U.S.A.* **109**:11025–11030.

Tamgüney G, Francis KP, Giles K, Lemus A, DeArmond SJ and Prusiner SB (2009) Measuring prions by bioluminescence imaging. *Proc. Natl. Acad. Sci. USA* **106**:15002–15006.

Telling GC, Haga T, Torchia M, Tremblay P, DeArmond SJ and Prusiner SB (1996) Interactions between wild-type and mutant prion proteins modulate neurodegeneration in transgenic mice. *Genes Dev.* **10**:1736-1750.

Trevitt CR and Collinge J (2006) A systematic review of prion therapeutics in experimental models. *Brain* **129**:2241-2265.

Watts JC, Giles K, Grillo SK, Lemus A, DeArmond SJ and Prusiner SB (2011) Bioluminescence imaging of Abeta deposition in bigenic mouse models of Alzheimer's disease. *Proc. Natl. Acad. Sci. USA* **108**:2528–2533.

Williamson RA, Peretz D, Pinilla C, Ball H, Bastidas RB, Rozenshteyn R, Houghten RA, Prusiner SB and Burton DR (1998) Mapping the prion protein using recombinant antibodies. *J. Virol.* **72**:9413-9418.

Zhu L, Ramboz S, Hewitt D, Boring L, Grass DS and Purchio AF (2004) Non-invasive imaging of GFAP expression after neuronal damage in mice. *Neurosci. Lett.* **367**:210-212.

FOOTNOTES

This work was supported by grants from the National Institutes of Health [AG02132, AG10770, and AG021601] as well as by a gift from the G. Harold and Leila Y. Mathers Charitable Foundation.

D.L. and K.G. contributed equally.
D.L. current address: Dana-Farber Cancer Institute, Boston, MA
Z.L. current address: Global Blood Therapeutics, Inc., South San Francisco, CA 94080
M.G. current address: Teva Pharmaceuticals, Netanya, Israel
B.M.S. current address: ELMEDTECH, San Francisco, CA 94123

JPET Fast Forward. Published on August 21, 2013 as DOI: 10.1124/jpet.113.205799
This article has not been copyedited and formatted. The final version may differ from this version.

LEGENDS FOR FIGURES

Figure 1. Potency of two independent batches of Compd B in reducing PrP^{Sc} levels in ScN2a-cl3 cells. (**A**) Batch provided by Dr. Doh-ura. (**B**) Batch synthesized commercially and used in subsequent studies. EC_{50} values are mean ± SEM, determined from *n*=4 (Doh-ura) or *n*=3 (commercial) independent experiments.

Figure 2. (**A**) A four-site pharmacophore model was generated containing one hydrogen-bond donor (blue), one-hydrogen bond acceptor (red) and two aromatic rings (yellow rings). From 274 active compounds screened previously, 150 fell within this four-site model, including Compd B (**B**).

Figure 3. Kaplan-Meier survival (**A, B**) and BLI (**C, D**) curves of Tg(*Gfap*-luc) mice (**A, C**) and Tg(MoPrP:*Gfap*-luc)4053 mice (**B, D**) infected with RML prions and treated with 110 mg/kg/day of Compd B beginning at 1 dpi. Compd B treatment (gray) extended survival by 90–100 d compared to untreated mice (black). Treatment with Compd B suppressed the BLI signal at 60 days (**C** inset), when infected untreated mice showed upregulation, which predicted efficacy of the compound. Bars under each graph indicate the initiation and duration of treatment.

Figure 4. Biochemical and neuropathologic analysis of Compd B–treated Tg(*Gfap*-luc) mouse brains. (**A**) Immunoblot of brain homogenates prepared from RML-infected Tg(*Gfap*-luc) mice without Compd B treatment (lane 1) and treated with 110 mg/kg/day of Compd B beginning at 1 dpi (lanes 2–9). Each lane shows brain homogenate from a single animal, whose incubation time is indicated. Samples were probed for protease-resistant PrP^{Sc} after PK digestion (upper panel); actin is shown as a

JPET Fast Forward. Published on August 21, 2013 as DOI: 10.1124/jpet.113.205799
This article has not been copyedited and formatted. The final version may differ from this version.

control (lower panel). Apparent molecular masses based on migrated protein standards are shown in kDa. (**B**) Conformational-stability curves of PrP^{Sc} in untreated (black) and Compd B–treated (gray), RML-infected Tg(*Gfap*-luc) mice. $GdnHCl_{1/2}$ values were 1.4 ± 0.2 M (n = 6) for the untreated group and 1.8 ± 0.3 M (n = 5) for the treated group, which were significantly different (p = 0.014). (**C–H**) Immunohistochemical analysis of brain sections from untreated (**C–E**, 112 dpi) and treated (**F–H**, 284 dpi) Tg(*Gfap*-luc) mice. H&E staining showed a small amount of vacuolation in the hippocampus in both untreated (**C**) and treated (**F**) mice. Immunostaining for PrP^{Sc} showed uniformly distributed and mildly intense PrP^{Sc} in virtually all regions of the brain of untreated mice (**D**). In contrast, PrP^{Sc} accumulated focally in treated mice (**G**), particularly in the thalamus, but also in the brainstem (not shown); no substantial PrP^{Sc} was found in the hippocampus or the neocortex. GFAP staining showed moderately intense astrocytic gliosis in virtually all regions of the brain of untreated mice (**E**) but minimal astrocytic gliosis was seen in the treated mice (**H**). Nc, neocortex; Hp, hippocampus; Th, thalamus. Bar in H represents 200 μm and applies to panels C–G.

Figure 5. Biochemical and neuropathologic analysis of Compd B–treated Tg(MoPrP:*Gfap*-luc)4053 mouse brains. (**A**) Immunoblots of brain homogenates prepared from prion-infected Tg(MoPrP:*Gfap*-luc)4053 mice without Compd B treatment (lane 1) and treated with 110 mg/kg/day of Compd B beginning at 1 dpi (lanes 2–13). Each lane shows brain homogenate from a single animal, whose incubation time is indicated. Samples were probed for PK-resistant PrP^{Sc} (upper panel); actin is shown as a control (lower panel). Apparent molecular masses based on migrated protein standards are shown in kDa. (**B**) Conformational-stability curves of PrP^{Sc} in untreated

JPET Fast Forward. Published on August 21, 2013 as DOI: 10.1124/jpet.113.205799
This article has not been copyedited and formatted. The final version may differ from this version.

(black) and Compd B–treated (gray) Tg(MoPrP:*Gfap*-luc)4053 mice. $GdnHCl_{1/2}$ concentrations were 1.4 ± 0.3 M (*n* = 6) for the untreated group and 1.7 ± 0.2 M (*n* = 6) for the treated group. (**C–H**) Immunohistochemical analysis of brain sections from untreated (**C–E**) and treated (**F–H**) Tg(MoPrP:*Gfap*-luc)4053 mice. H&E staining showed mild vacuolation in untreated (**C**) and treated mice (**F**). Immunostaining for PrP^{Sc} showed intense, uniformly distributed PrP^{Sc} throughout the brain of untreated mice (**D**) and multifocal patches of PrP^{Sc} accumulation in treated mice (**G**). GFAP staining showed intense astrocytic gliosis, particularly in the hippocampus, of untreated mice (**E**), but multifocal, moderately intense astrocytic gliosis resembling the patchy distribution of PrP^{Sc} in treated mice (**H**). Nc, neocortex; Hp, hippocampus; Th, thalamus. Bar in H represents 200 μm and applies to panels C–G.

Figure 6. Survival, biochemical, and pathological analyses of Tg(MHu2M,M111V,M165V,E167Q)1014 mice infected with sCJD prions. (**A**) Kaplan-Meier survival curve of Tg1014 mice infected with sCJD prions and treated with 110 mg/kg/day of Compd B (gray) beginning at 1 dpi. Untreated mice are shown as controls (black). No extension in survival was observed. (**B**) Immunoblot of brain homogenates prepared from the sCJD(MM1) inoculum (lane 1), prion-infected Tg1014 mice without Compd B treatment (lanes 2 and 3), and prion-infected Tg1014 mice treated with 110 mg/kg/day of Compd B beginning at 1 dpi (lanes 4 and 5). Samples were probed for PK-resistant PrP^{Sc}. Apparent molecular masses based on migrated protein standards are shown in kDa. (**C–H**) Immunohistochemical analysis of brain sections from untreated (**C–E**) and treated (**F–H**) Tg1014 mice. H&E staining showed robust vacuolation in untreated (**C**) and treated mice (**F**). Immunostaining for PrP^{Sc} showed intense, uniformly

JPET Fast Forward. Published on August 21, 2013 as DOI: 10.1124/jpet.113.205799
This article has not been copyedited and formatted. The final version may differ from this version.

distributed PrP^{Sc} throughout the brains of both untreated (**D**) and treated mice (**G**). GFAP staining showed severely intense astrocytic gliosis, particularly in the hippocampus, of untreated mice (**E**) and treated mice (**H**). Nc, neocortex; Hp, hippocampus; Th, thalamus. Bar in H represents 200 μm and applies to panels C–G.

Figure 7. Kaplan-Meier (**A, B**) and BLI (**C, D**) curves of Tg(*Gfap*-luc) mice infected with RML prions and treated with 110 mg/kg/day of Compd B (gray) beginning at 60 dpi (**A, C**) or 78 dpi (**B, D**). Untreated mice are shown as controls (black). Delayed treatment resulted in shorter extensions in survival time, compared to Tg(*Gfap*-luc) mice treated with Compd B beginning at 1 dpi (see Figure 3A). Bars under each graph indicate the initiation and duration of treatment.

JPET Fast Forward. Published on August 21, 2013 as DOI: 10.1124/jpet.113.205799
This article has not been copyedited and formatted. The final version may differ from this version.

Table 1. EC_{50} values of biaryl amide analogs of Compd B in ScN2a-cl3 cells.

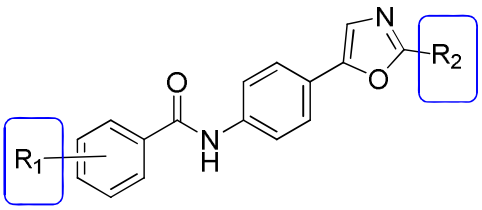

Compound no.	R_1	R_2	EC_{50} (μM)*
1	4-pyridyl (in place of R_1-phenyl)	H	Inactive
2	H	H	0.64 ± 0.07
3	4-MeO	H	0.12 ± 0.01
4	4-Cl	H	0.12 ± 0.07
5	3-MeO,4-Me	H	0.16 ± 0.03
6	2,4-diF	H	0.34 ± 0.06
7	4-CN	Me	0.51 ± 0.11
8	4-$OCHF_2$	Me	0.19 ± 0.05
9	2-$NCCH_2S$	Me	Inactive
10	2-F		0.30 ± 0.01
11	3-F		0.54 ± 0.19
12	4-F		0.08 ± 0.02
13	2,4-diF		0.23 ± 0.05
14	4-Cl		0.10 ± 0.03
15	4-$MeOCH_2CH_2O$		0.06 ± 0.02
16	3-CN		0.36 ± 0.15
17	4-CN		0.54 ± 0.13
18	3-Me		0.39 ± 0.08

** Average ± standard deviation of three independent runs.*

Table 2. Pharmacokinetic parameters of Compd B and analogs.*

Compound	Brain Exposure		Plasma Exposure		Microsomal Stability	
	C_{max} (µM)	AUC_{last} (µM*h)	C_{max} (µM)	AUC_{last} (µM*h)	$t_{1/2}$ in min (% remaining after 60-min incubation)	
					Mouse	Human
Compd B	0.46 ± 0.16	1.23 ± 0.15	0.83 ± 0.38	2.36 ± 0.25	15 (6)	57 (49)
1	0.31 ± 0.01	0.08 ± 0.01	0.34 ± 0.01	0.47 ± 0.02	15 (6)	>60 (80)
2	0.36 ± 0.08	0.94 ± 0.30	0.55 ± 0.05	1.54 ± 0.44	12 (3)	>60 (60)
3	0.02 ± 0.00	0.03 ± 0.04	0.04 ± 0.04	0.15 ± 0.11	7 (0.1)	>60 (49)
4	0.08 ± 0.08	0.14 ± 0.11	0.05 ± 0.06	0.08 ± 0.08	11 (2)	>60 (70)
5	0.89 ± 0.47	1.97 ± 0.43	1.36 ± 0.76	3.13 ± 0.87	20 (12)	>60 (51)
6	0.13 ± 0.03	0.26 ± 0.07	0.11 ± 0.04	0.26 ± 0.07	16 (7)	>60 (70)
7	0.05 ± 0.04	0.18 ± 0.12	0.05 ± 0.04	0.18 ± 0.10	16 (7)	9 (0.9)
8	0.03 ± 0.00	0.01 ± 0.00	0.04 ± 0.01	0.06 ± 0.01	5 (0.2)	9 (1)
9	0.97 ± 0.03	2.35 ± 0.28	3.77 ± 0.87	7.86 ± 1.46	29 (24)	>60 (54)
10	6.12 ± 1.75	16.8 ± 0.52	2.53 ± 0.85	7.59 ± 0.76	21 (14)	>60 (80)
11	1.28 ± 0.11	5.97 ± 0.83	0.87 ± 0.12	3.74 ± 0.04	21 (15)	>60 (81)
12	1.14 ± 0.03	4.83 ± 0.95	0.71 ± 0.06	3.13 ± 0.67	17 (9)	>60 (81)
13	2.74 ± 0.65	13.5 ± 0.23	1.20 ± 0.78	6.10 ± 0.26	18 (11)	>60 (87)
14	0.46 ± 0.38	0.88 ± 0.32	0.16 ± 0.13	0.33 ± 0.10	7 (0.4)	>60 (74)
15	0.28 ± 0.17	0.48 ± 0.14	0.10 ± 0.06	0.30 ± 0.06	11 (3)	36 (33)
16	5.16 ± 2.93	18.7 ± 5.69	6.39 ± 3.10	23.9 ± 6.23	>60 (70)	>60 (94)
17	2.86 ± 0.35	6.61 ± 0.01	1.54 ± 0.56	4.09 ± 0.61	24 (18)	>60 (79)
18	1.09 ± 0.11	4.22 ± 0.71	1.05 ± 0.11	3.90 ± 0.89	25 (20)	>60 (63)

** Brain and plasma exposure were measured in vivo after a single dose of 10 mg/kg administered by oral gavage. Microsomal stability was measured in vitro in mouse and human microsomal preparations. C_{max}, maximum peak drug concentration; AUC_{last}, area under the time concentration curve from time zero to time of last measurable concentration; $t_{1/2}$, half-life.*

JPET Fast Forward. Published on August 21, 2013 as DOI: 10.1124/jpet.113.205799
This article has not been copyedited and formatted. The final version may differ from this version.

Table 3. Incubation periods for prion-infected mice treated with Compd B.

Mouse line	Inoculum	Dose (mg/kg/day)	Treatment started (dpi)	Mean incubation period ± SEM (days)	n/n_0*
Tg(*Gfap*-luc)	RML	0	n/a	108 ± 1	8/8
Tg(*Gfap*-luc)	RML	110	1	219 ± 21	10/10
Tg(*Gfap*-luc)	RML	110	60	182 ± 9	9/9
Tg(*Gfap*-luc)	RML	110	78	163 ± 14	9/9
Tg(MoPrP:*Gfap*-luc)4053	RML	0	n/a	52 ± 2	15/15
Tg(MoPrP:*Gfap*-luc)4053	RML	110	1	143 ± 7	12/12
Tg(MHu2M,M111V,M165V,E167Q)1014	sCJD	0	n/a	80 ± 1	13/13
Tg(MHu2M,M111V,M165V,E167Q)1014	sCJD	110	1	78 ± 1	5/5

*n, *number of ill mice;* n_0, *number of inoculated mice.*

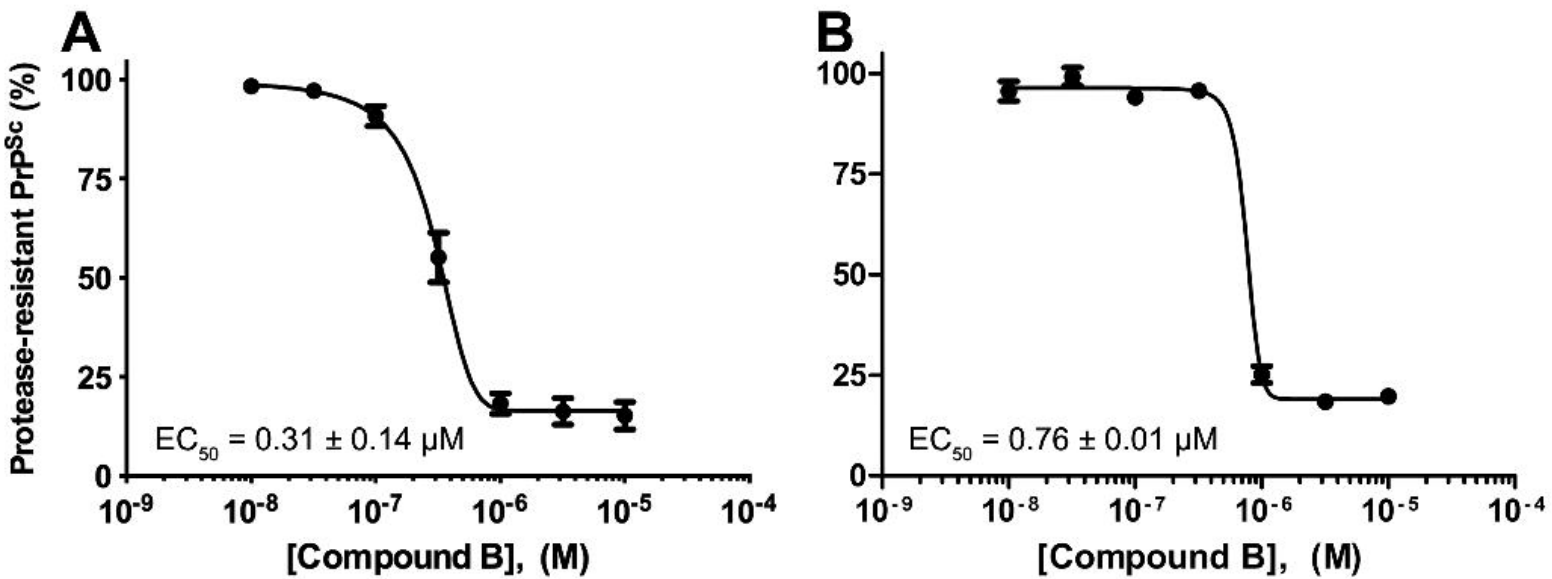
A
Protease-resistant PrPSc (%)
100
75
50
25
0
EC50 = 0.31 ± 0.14 μM
10-9
10-8
10-7
10-6
10-5
10-4
[Compound B], (M)
B
100
75
50
25
0
EC50 = 0.76 ± 0.01 μM
10-9
10-8
10-7
10-6
10-5
10-4
[Compound B], (M)

FIGURE 1

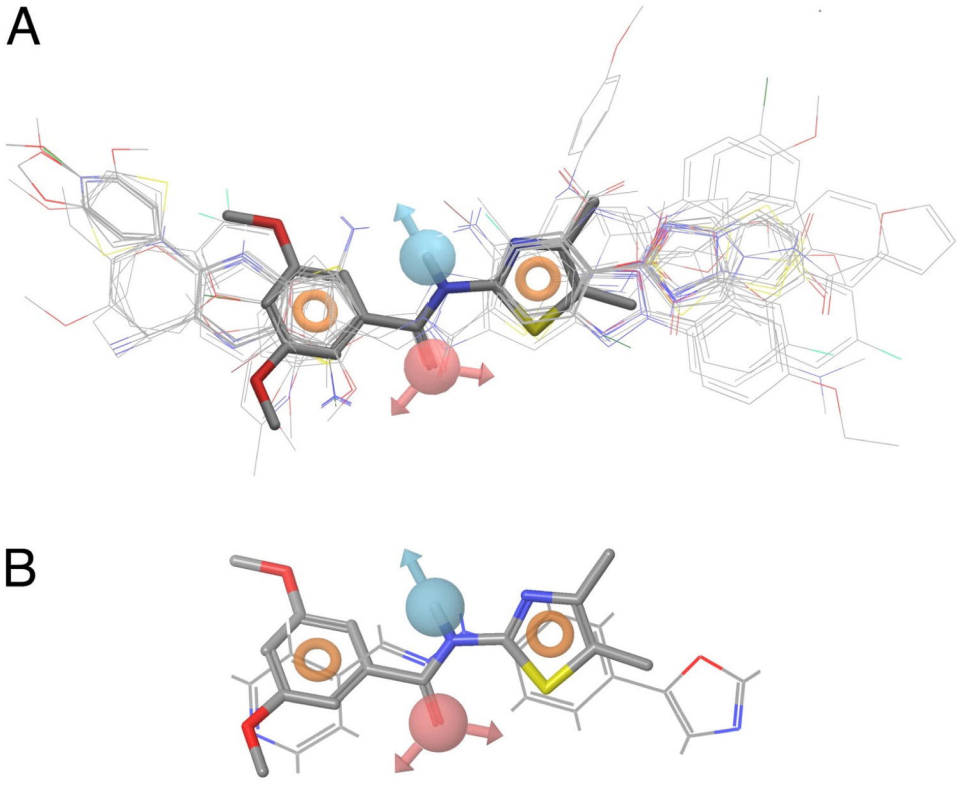

FIGURE 2

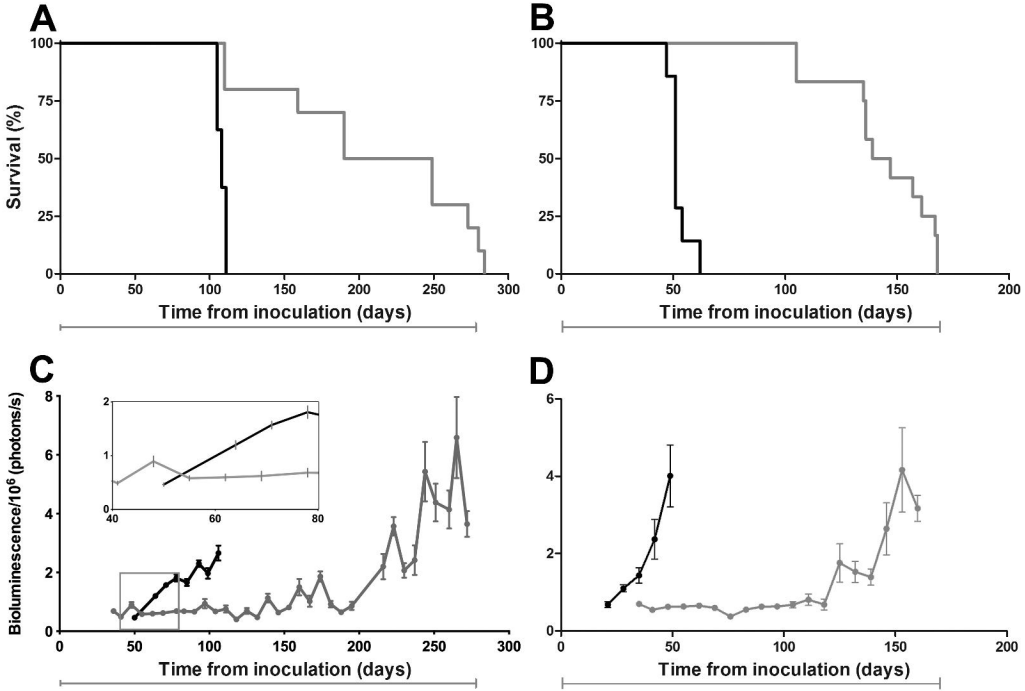
A
B
C
D
Survival (%)
Time from inoculation (days)
Bioluminescence/10^6 (photons/s)
Time from inoculation (days)
Time from inoculation (days)
Time from inoculation (days)

FIGURE 3

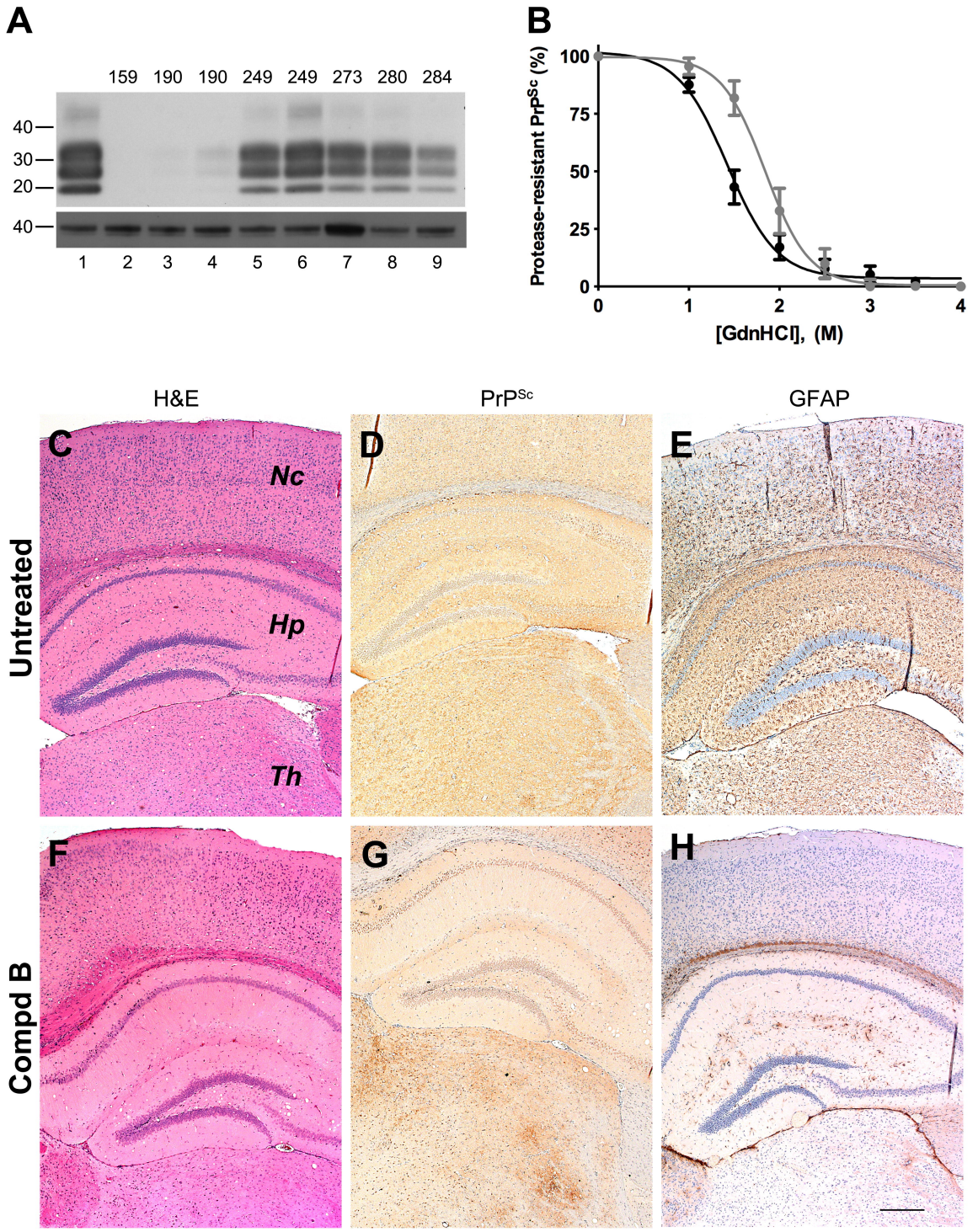
A
159 190 190 249 249 273 280 284
40
30
20
40
1 2 3 4 5 6 7 8 9
B
Protease-resistant PrPSc (%)
100
75
50
25
0
0 1 2 3 4
[GdnHCl], (M)
H&E
PrPSc
GFAP
Untreated
Compd B
C
Nc
Hp
Th
D
E
F
G
H

FIGURE 4

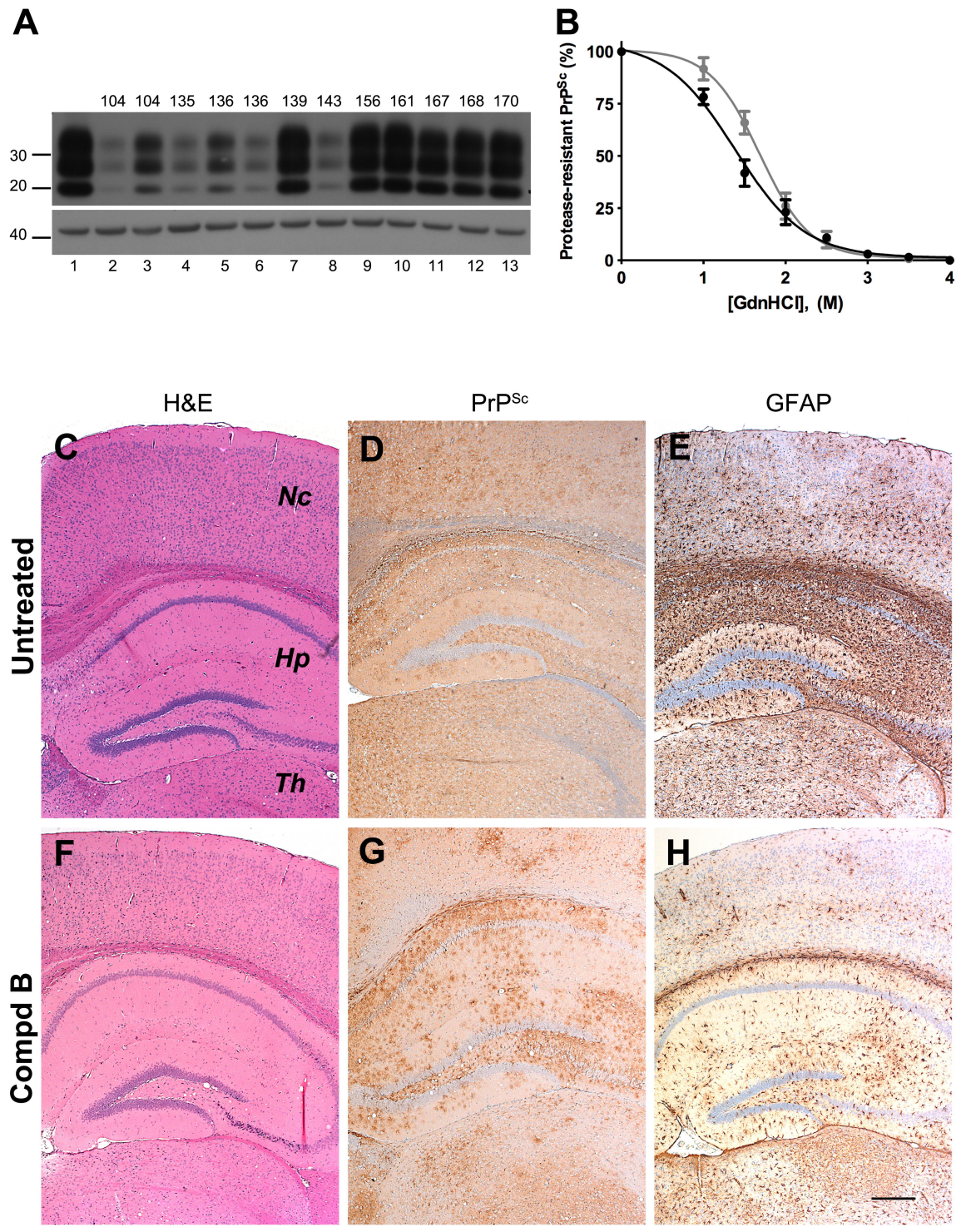
A
104 104 135 136 136 139 143 156 161 167 168 170
30
20
40
1 2 3 4 5 6 7 8 9 10 11 12 13
B
Protease-resistant PrPSc (%)
100
75
50
25
0
0 1 2 3 4
[GdnHCl], (M)
H&E
PrPSc
GFAP
Untreated
Compd B
C
D
E
F
G
H
Nc
Hp
Th

FIGURE 5

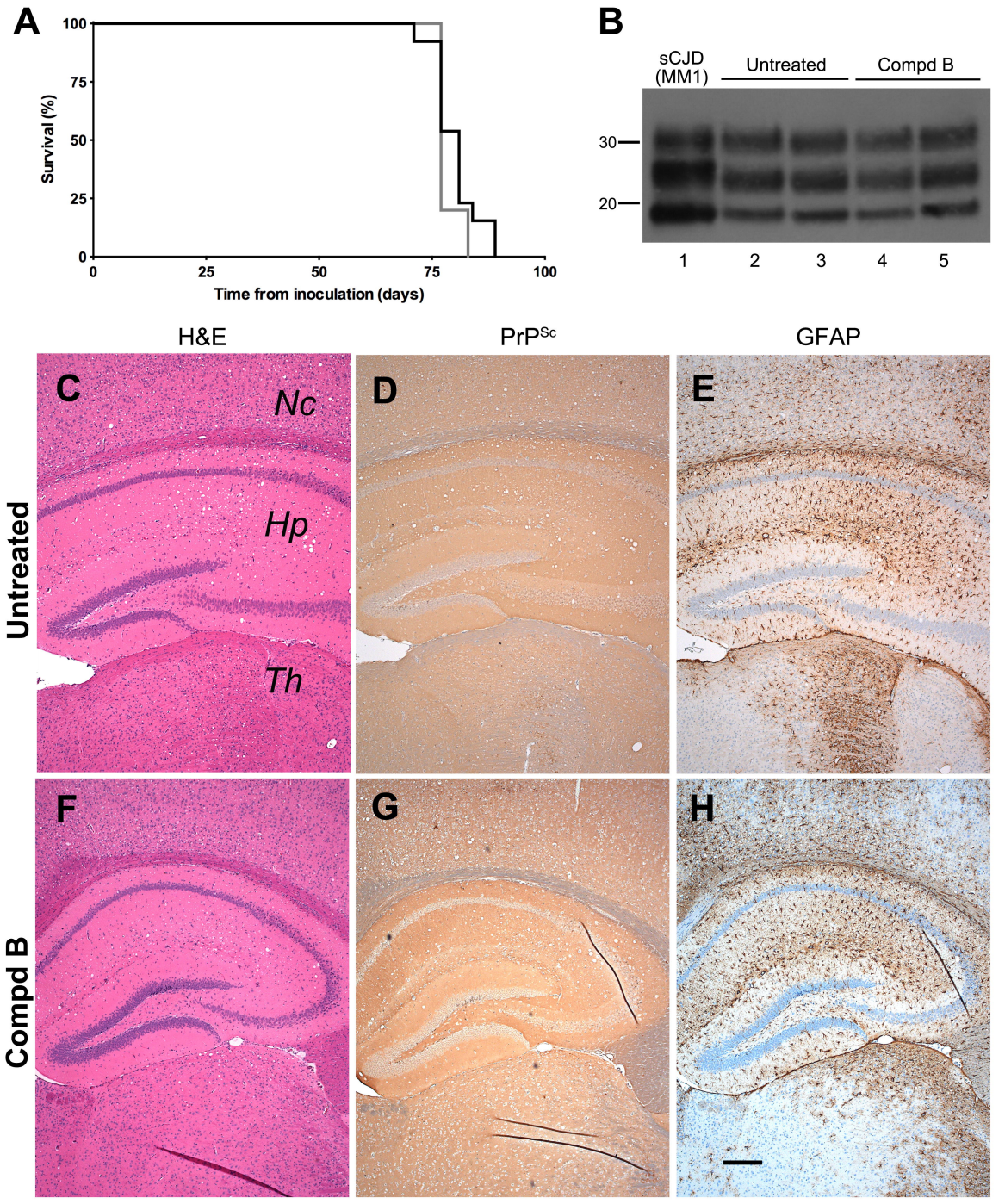
A
100
75
50
25
0
Survival (%)
0
25
50
75
100
Time from inoculation (days)
B
sCJD (MM1)
Untreated
Compd B
30
20
1
2
3
4
5
H&E
PrP^Sc
GFAP
Untreated
Compd B
C
Nc
Hp
Th
D
E
F
G
H

FIGURE 6

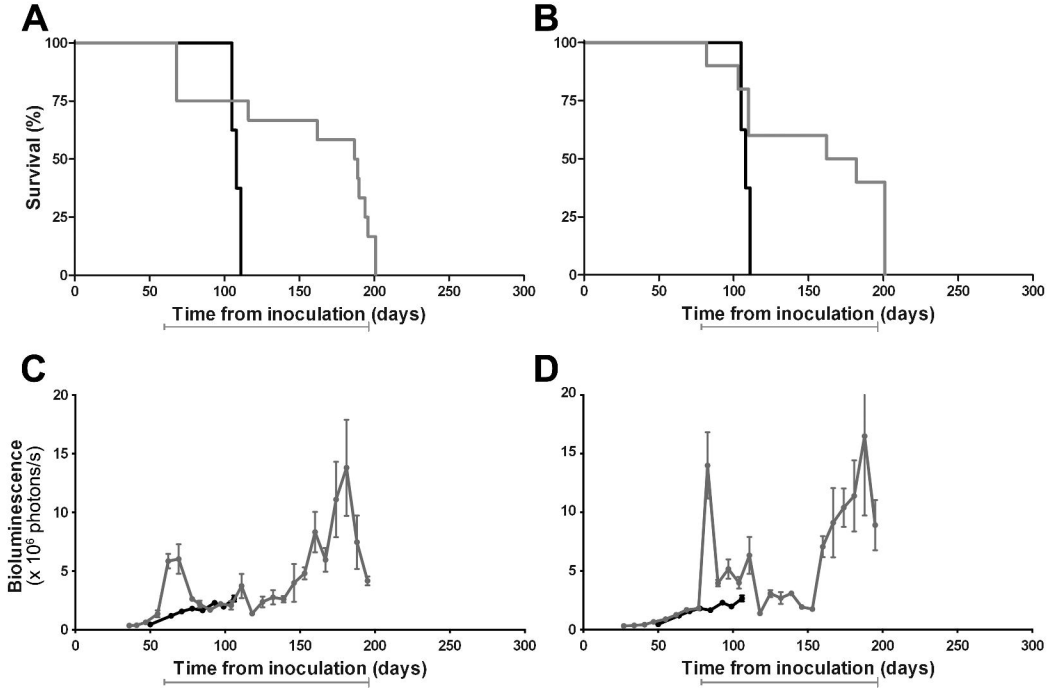
A
B
C
D
Survival (%)
Time from inoculation (days)
Bioluminescence
(x 10^6 photons/s)
0
25
50
75
100
150
200
250
300
5
10
15
20

FIGURE 7